Measurement of $2\beta 2\nu$ Half-Life of Zr^{96} with NEMO-3 Detector

Matthew Kauer
Department of Physics and Astronomy
University College London

Abstract
This report details the progress made in the past 8 months towards two separate goals. The first and currently most important goal is the analysis of the $2\beta 2\nu$ decay of Zr96. This analysis will lead to a measurement of the $2\beta 2\nu$ half-life of Zr96. The second object of focus is the design study of the SuperNEMO calorimeter and calibration techniques.

1 Introduction

Neutrino physics has continued to gain momentum ever since Wolfgang Pauli's proposal in 1939 that beta decay is accompanied by a very small particle, the neutrino [**1**]. This idea was proposed to explain why the beta decay spectrum was continues and not a delta function at Q(β). The idea that the neutrino was carrying away some of this energy was a breakthrough, despite Pauli's feelings that, "I did a terrible thing – invented a particle that can't be detected." The Standard Model (SM) predicts that neutrinos are massless Dirac particles. Bruno Pontecorvo proposed in 1957 [**2**] that if neutrinos had non-zero mass, they could oscillate between flavor eigenstates and this was soon indicated by Ray Davis's solar neutrino disappearance experiment.

Today we know that neutrinos oscillate between flavors due to the mixing of their mass and flavor eigenstates [**3**]. This can only happen if the neutrinos have non-zero mass. The neutrino mixing angles and mass-squared differences have been measured repeatedly and are now constrained. The big remaining questions are whether the neutrino is a Dirac particle or Majorana particle and what is the absolute mass scale of the neutrinos. The most sensitive experiment for determining whether the neutrino is its own anti-particle is a double beta decay experiment where the neutrinos annihilate and the full Q($\beta\beta$) of the decay is split between the two electrons [**4**]. Neutrinoless double beta decay ($2\beta 0\nu$) is a lepton number violating process and if proven true would require some drastic changes to the Standard Model. Coincidentally, the activity of the $2\beta 0\nu$ decay mode also provides a direct measurement of the effective electron neutrino mass.

2 Double Beta Decay Theory

In 1935, Maria Gopert-Mayer proposed the possibility of double beta decay [**5**] within a nucleus. For even-A nuclei due to the non-zero pairing term in the semi-empirical mass formula (SEMF), there are two stability curves. The even-even (even-A and even-Z) nuclei lie on the lower energy curve, while the odd-odd nuclei are on the higher energy curve. Thus for even-even nuclei the nearest odd-odd neighbor nucleus will almost always have a higher mass and therefore single beta decay is not possible, but this means that double beta decay is a possibility. This is a lepton number conserving process and is allowed by the Standard Model [**6**].

$$(A, Z) \dashrightarrow (A, Z+2) + e^- + e^- + \bar{\nu}_e + \bar{\nu}_e$$

Then Majorana proposed that neutrinos could be their own anti-particles [**7**]. This lead to Furry's conclusion [**8**] that neutrinoless double beta decay is a possible mode if the neutrinos have mass (figure 2.1).

$$(A,\ Z) \dashrightarrow (A,\ Z+2) + e^- + e^-$$

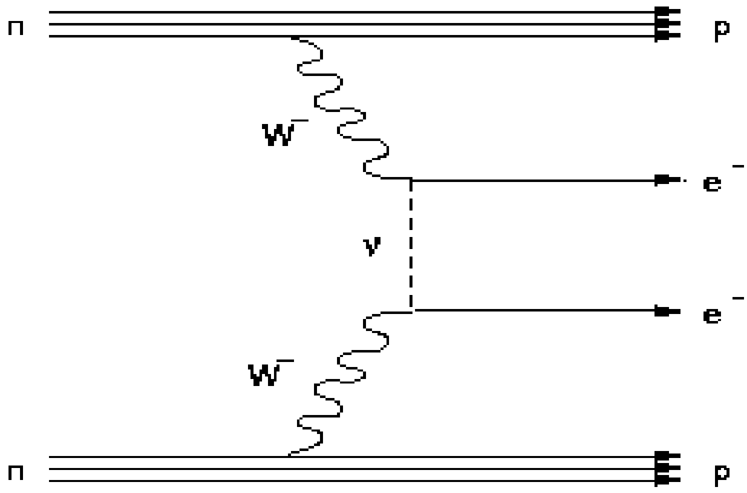

Figure 2.1 Feynman diagram for $2\beta0\nu$

To gain further insight, the above Feynman diagram can be split into two separate processes. The top part of the diagram can be shown as a neutron decaying into a proton, electron, and Majorana neutrino. The bottom part of the Feynman diagram can be shown as a neutron absorbing a Majorana neutrino and then going to a proton and electron.

$$n \dashrightarrow p + e^-_L + \nu_e{}^M{}_R \qquad (A)$$

$$\nu_e{}^M{}_L + n \dashrightarrow p + e^-_L \qquad (B)$$

This process requires that the right-handed Majorana neutrino from (A) change into a left-handed neutrino so that it can be absorbed in reaction (B). If the Majorana neutrino has mass, a frame of reference can be chosen that transforms the right-handed neutrino to a left-handed neutrino. Furthermore, the mass of the neutrino is proportional to the amplitude of reaction (B). Thus, the contribution of the neutrino exchange to the $2\beta0\nu$ amplitude is proportional to the neutrino mass [**9**]. There are other mechanisms to explain neutrinoless double beta decay but the above mechanism is the most favored. The half-life for $2\beta2\nu$ mode is given by:

$$\left[T_{1/2}{}^{2\nu}\right]^{-1} = G^{2\nu}\ |M_{2\nu}|^2$$

The study of the $2\beta2\nu$ channel is an important prelude to the study of the $2\beta0\nu$ channel. A precision measurement of an isotope's $2\beta2\nu$ half-life leads to a more accurate description of the matrix elements and also provides the spectrum shape of the energy distribution. The main background to the $2\beta0\nu$ channel is the $2\beta2\nu$ channel. A better understanding of $2\beta2\nu$ will lead to a better measurement of $2\beta0\nu$. The half-life for the $2\beta0\nu$ channel is inversely proportional to the effective neutrino mass as shown below:

$$\left[T_{1/2}{}^{0\nu}\right]^{-1} = G^{0\nu}\ |M_{0\nu}|^2\ \langle m_{\beta\beta}\rangle^2$$

Where 'G' is the phase-space factor and 'M' is the nuclear matrix element. For the neutrinoless mode, '$m_{\beta\beta}$' is the effective Majorana neutrino mass. The largest uncertainty in the effective mass measurement comes from the matrix elements.

3 NEMO-3 Detector

3.1 General Overview

NEMO-3 is a continuation of the NEMO-1 and NEMO-2 experiments. Experience and proof of concept from NEMO-1 and NEMO-2 lead to the proposal and funding for NEMO-3. The NEMO-3 detector is a cylindrical detector, divided into 20 sectors and each sector containing 7 thin source foils. The detector is about 6 meters in diameter and 3 meters in height, not including the passive shielding. A total of 10kg of source foils are spread through the center of a Geiger cell tracker with a calorimeter surrounding the tracker and the whole detector bathed in a uniform magnetic field. The detector is located in a tunnel in the Laboratoire Souterrain de Modane on the French-Italian border. The detector has 1700 meters of rock (4800 MWE) above it acting as passive shielding against cosmic rays. This decreases the flux by a factor of approximately one million.

3.2 Tracker Volume

The source foils have 9 vertical drift cell layers on either side acting in Geiger mode. 4 layers are close to the foil to improve vertex resolution, 2 layers in between the foil and calorimeter, and 3 layers close to the calorimeter. A uniform, 25 gauss magnetic field permeates the detector and tracker region to provide electron-positron separation.

3.3 Calorimeter

The calorimeter is built up of ~2000 photomultiplier tubes (PMT's) on either side of the tracker volume, coupled via a plastic light-guide to polystyrene doped with PTP and POPOP to cause scintillation. The scintillators are wrapped in Mylar to reflect escaping light back to the PMT, thus greatly improving the energy resolution. The energy resolution of the calorimeter is critical to the separation between the $2\beta2\nu$ and $2\beta0\nu$ spectra and was experimentally measured to be ~14% dE/E full width at half max (FWHM) at 1MeV (~6% dE/E at 1σ at 1MeV). The timing of the calorimeter is also important for time-of-flight (TOF) information which triggers the Geiger cells into operation.

3.4 Source Foils

NEMO-3 accommodates 10kg of double-beta decay isotopes. Most of the isotopes went through an enrichment and purification process. There are 8 different isotopes being used in total, and distributed throughout the 20 sectors of the detector. The foil thickness was specifically chosen so that the energy loss effects would contribute to the energy resolution less than what was achievable with the calorimeter.

3.5 Backgrounds

The success of NEMO-3 strongly depends upon the ability to efficiently tag background events and accurately identify and measure the background sources that are contributing to the data. Because the $2\beta2\nu$ spectrum is continuous, it is contaminated by many low and high energy backgrounds. Backgrounds with Q(β) close to the Q($\beta\beta$) of the isotope under study are the most harmful to the $2\beta0\nu$ analysis because these backgrounds can easily mimic $2\beta0\nu$ events. The major backgrounds to the $2\beta0\nu$ analysis are Bi214 and Tl208 found in the natural decay chains of U238 and Th232. Both Bi214 and Tl208 have a high Q(β) of 3.270 and 4.992 MeV respectively.

3.5.1 Internal Background

Internal backgrounds are classified as impurities within the source foil that mimics double-beta decay. There are 3 main contributing mechanisms that mimic double-beta decay. There can be a beta decay accompanied by an internal conversion electron, a beta decay going to Moller scattering, and a beta decay accompanied by Compton scattering. All the source foils were repeatedly purified to minimize radioactive contaminants.

3.5.2 External Backgrounds

The majority of external backgrounds are crossing electrons but these are quickly eliminated by the TOF information. The other significant background is characterized by a crossing gamma which interacts with the source foils. There are 3 main mechanisms that mimic double-beta decay. The gamma can go to pair production, double Compton scattering, or Compton plus Moller scattering. External backgrounds come from a number of sources including the detector support structure, the PMT's, the wires in the tracker, radon in the air, the surrounding rock and cosmics. All support structure materials, tracker and calorimeter components were specially chosen to minimize the radioactive impurities. A combination of water, wood, iron, and paraffin wax was used as passive shielding to block out gammas and neutrons from the surrounding air and rock.

3.5.3 Radon

Radon is a danger to all low-background counting experiments including NEMO-3. Radon is a noble gas that diffuses into everything including liquids and solids. It is continuously expelled as a daughter decay from the U238 chain from the surrounding rock and has a long half-life $\sim$4 days. The dangerous contribution from radon is its daughter isotope Bi214 which has a high Q(β) which can easily mimic the 2β decay channels. Radon activity can be identified by looking at its daughter isotope but this can be tricky because of broken equilibrium and the detector's exposure time to the radon environment. Fortunately for phase-2 of the detector runtime, a radon purification facility was put in place to force clean air into a tent surrounding the detector, thus expelling the radon out and minimizing exposure. The measured radon activity for phase-1 is $\sim$800 Bq. The measured activity for phase-2 was $\sim$0 Bq proving the significance of the forced air purification facility [**10**].

4 Analysis

The detector description is written with GEANT 3. Simulations are done for all the isotopes and backgrounds. All the Monte Carlo (MC) and data are reconstructed and analyzed with dedicated software packages.

4.1 Monte Carlo

The NEMO-3 detector description was written with GEANT to accurately describe all the parts and components of the detector. All the $2\beta2\nu$, $2\beta0\nu$, and single β backgrounds are simulated with genBB in union with GEANT [**11**]. The genBB software simulates the decay processes and energy spectra while GEANT then simulates any Compton scattering, Moller scattering, or pair production, ...etc for the different isotopes and backgrounds.

4.2 Data Reconstruction

The MC and data are reconstructed with a software package called NEMOR, which fits a track to the Geiger cell hits and reconstructs the event vertex, the energies, the timings, efficiency degradation, and others [**10**]. When the reconstruction is complete, NEMOR outputs a *.root file which is used with the ROOT analysis software package.

4.3 Analysis Software

There are a few different software packages being used by various people in the NEMO collaboration. Some people are writing their own software, while others are developing a standard package that can be used by all collaborators to maintain consistency throughout the data analysis. The UK team has developed a standard package called “rootana”, written in C++ and uses the ROOT framework [10]. It was decided that I should utilize this software.

The rootana package functions by looping over all events (data and MC) and cutting out events that do not pass the user specified parameters, for instance, having a total energy greater than 400 keV. The MC is time normalized and weighted by its respective activities which are pre-set by the user. Background MC is subtracted from the data and the remainder is fit with the appropriate $2\beta2\nu$ or $2\beta0\nu$ spectrum shape for the isotope under study. The total number of events within the fit is proportional to the activity of the isotope and efficiency of the detector.

4.4 Zr96 Analysis

This analysis is being done to measure the $2\beta2\nu$ half-life of the Zr96 isotope. There are a number of steps that must be done before the actual analysis of the $2\beta2\nu$ channel can be done. The MC must be generated. The data and MC must be reconstructed. The internal and external backgrounds must be modeled so that the activities are predicted. Appropriate event selection criteria (cuts) must be decided to maximize efficiency and signal to noise ratio.

4.4.1 Monte Carlo and Reconstruction

All the MC had already been generated but slight updates and modifications did occur. Most of the MC had been reconstructed but there was some new MC that required reconstruction as well as updated versions of the reconstruction software which required that all the MC be reconstructed again. This was a fairly simple process that just involved passing the raw MC data to the reconstruction software and waiting for the output files.

4.4.2 Internal Backgrounds

Single beta decay going to Moller scattering is most likely the dominant process contributing to internal backgrounds and is very hard to distinguish from real double-beta decay. An accurate knowledge of the background contaminants and their activities is vital to the success of the experiment. Determining the internal backgrounds is done in two parts. A sample of the source is measured by a High Purity Germanium (HPGe) detector to provide a measurement or at least a limit on the activity of the contaminant. Germanium's superb energy resolution and gamma efficiency makes it great for measuring nuclear decay spectra of gamma emitters. Because the sample being measured has some mass and volume, alphas and betas lose either too much energy or all energy before being detected by the Germanium. For this reason, HPGe detectors are only used to identify the strong gamma lines of radioactive isotopes.

We use the HPGe data as a rough estimate but it is important to measure the backgrounds with the detector itself. Since the backgrounds are beta and gamma emitters, it is wise to look in the single electron and electron plus gamma channels. Selection cuts are made to single out these channels and the isotope's activities are left as free parameters and fit to the data.

4.4.3 External Backgrounds

External backgrounds are a bit trickier but the process of determining background activities is somewhat the same. There is one sector of the NEMO-3 detector fitted with high purity copper foils instead of double-beta sources for exactly the purpose of measuring the external backgrounds. The internal backgrounds of the copper are small and well understood, therefore we can fit the the copper data leaving only the external backgrounds as free parameters. Different channels are selected and MC is compared to data and background activities are adjusted until MC and data are in agreement. Comparing different channels has proved to be very important in distinguishing between real backgrounds and fake backgrounds that coincidentally fit the data. A fake background might fit the data in one channel but will misrepresent the spectrum shape in another channel, while a real background will fit the data in both channels. This is an excellent cross-check to make sure fake backgrounds are not being added in to explain the data.

4.4.4 Zr96 $2\beta2\nu$ Measurement

The first part of my analysis was to determine the Zr96 $2\beta2\nu$ half-life using pre-existing internal and external background models. Victor Tretyak's internal and external background models were used [**12**]. It is important to note at this point that the data is split into 2 phases. This is because the radon levels were high in phase-1 and the radon purification facility wasn't in place until the beginning of phase-2. This means there are actually 2 external background models. One for phase-1 and one for phase-2. The models include the background isotopes present and associated activities. Victor Tretyak has also done a $2\beta2\nu$ half-life measurement for Zr96 and his measurement provides a good cross-check for my analysis.

The next step is to create a selection criteria. This is accomplished by writing C++ code to loop over all the events and exclude (or cut) out events that do not meet the criteria. An important part of the analysis is choosing correct cuts and understanding the physics behind the cuts.

4.4.4.1 Selection Criteria

- Cut on the physical location of the event, checking that it is from the Zr96 foil. This means finding the angle between the X-axis and the event radius and calculating which sector the event happened in. In the case of Zr96, the source only occupies half of the foil so a Z position cut is also made to check that the event came from the Zr96 side of the foil.
- Require the event to have 2 reconstructed tracks both with negative curvature and 2 corresponding scintillator hits with a threshold of 200keV.
- Check that no Geiger cell hits are on the opposite side of the foil where the event vertex is. This makes sure that a single beta decay did not happen close to the foil and pass through the foil causing Moller scattering.
- Require the 2 reconstructed track intersections with the foil be less than 2cm apart in X and Y-axis, and less than 4cm in the Z-axis.
- Require that one of the first 2 layers of the Geiger chamber were hit. This helps reduce the accepted events that actually didn't take place on the foil but near it.
- Check the internal and external hypothesis. This uses the time-of-flight (TOF) data to calculate the probability that the event happened within the foil or outside the foil.
- Require that only 2 scintillators have deposited energy. This reduces the number of events with gamma's in them. (note that the 10cm thick scintillator blocks only have a 50% interaction probability for 500 keV gammas)
- Check for delayed Geiger hits after and event. This helps reduce the number events that are not real and have a short half-life alpha decay. Bi214 -> Po214 via a beta decay and then Po214 -> Pb210 via an alpha decay. Po214 has a half-life of 163 microSec.

4.4.4.2 Results

The MC has all been reconstructed. Appropriate internal and external backgrounds models have been realized. Event selection criteria has been decided and written into the analysis code. It is now time to utilize the "rootana" package that will subtract the backgrounds from the data and fit the remainder with the Zr96 $2\beta2\nu$ spectrum, leaving the activity as the free parameter. There are two results, one for phase-1 and for phase-2 (figure 4.3 and 4.4).

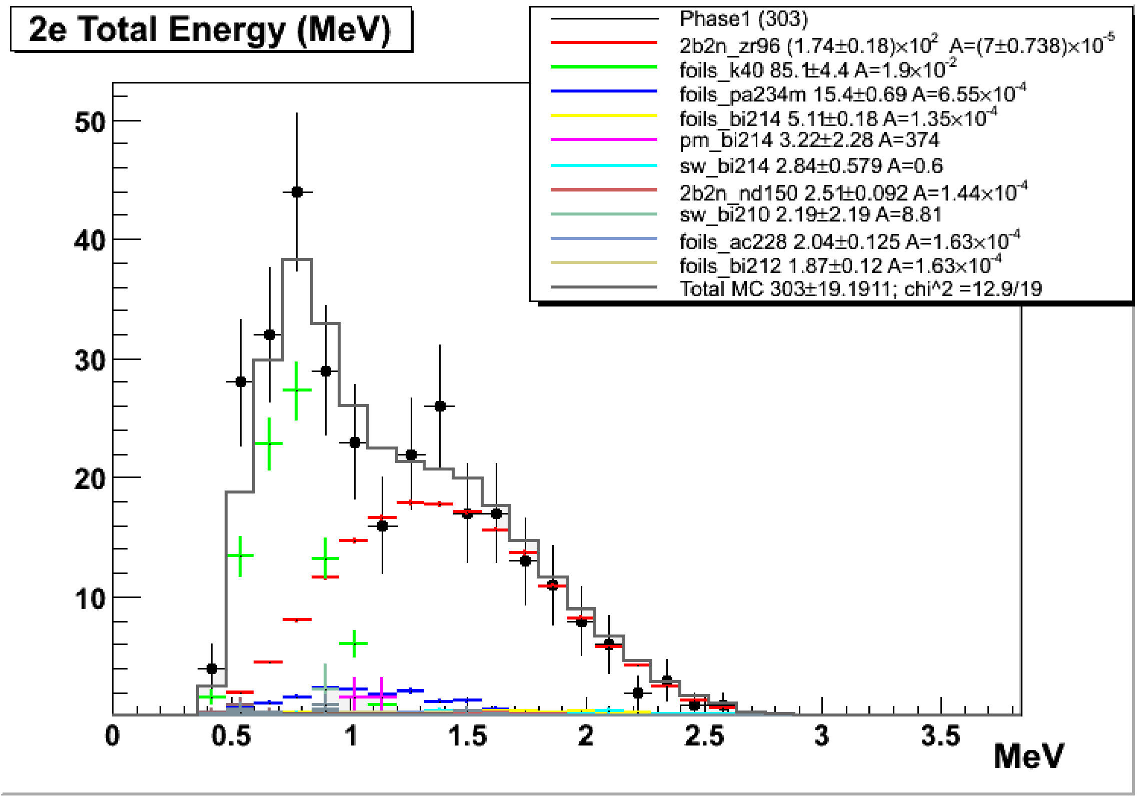

Figure 4.3 Phase-1 Analysis
This is a plot of the summed energy of the two electrons emitted from the source.

The data is shown as black dots with error bars, the sum of all MC is the solid black line, the Zr96 MC fit to the spectrum are the red points, and the other colored points are the various backgrounds. This scheme will hold true for all the other plots shown for the Zr96 analysis.

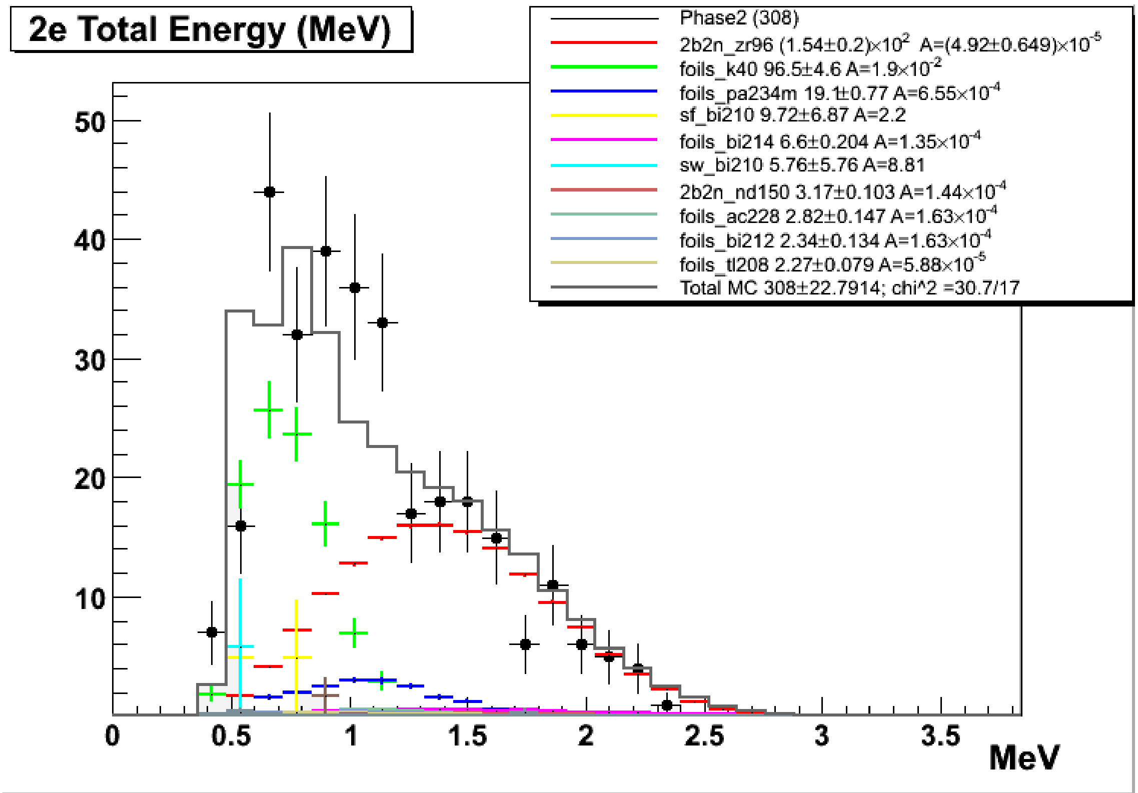

Figure 4.4 Phase-2 Analysis
This is a plot of the summed energy of the two electrons emitted from the source.

The phase-1 analysis fit the spectrum to a half-life of 1.85+/-0.20e19 years and phase-2 yielded a half-life of 2.63+/-0.35e19 years. It is also useful to compare angular distributions of the data and MC (figure 4.5). One method for distinguishing between different $2\beta0\nu$ mechanisms is with their angular distributions.

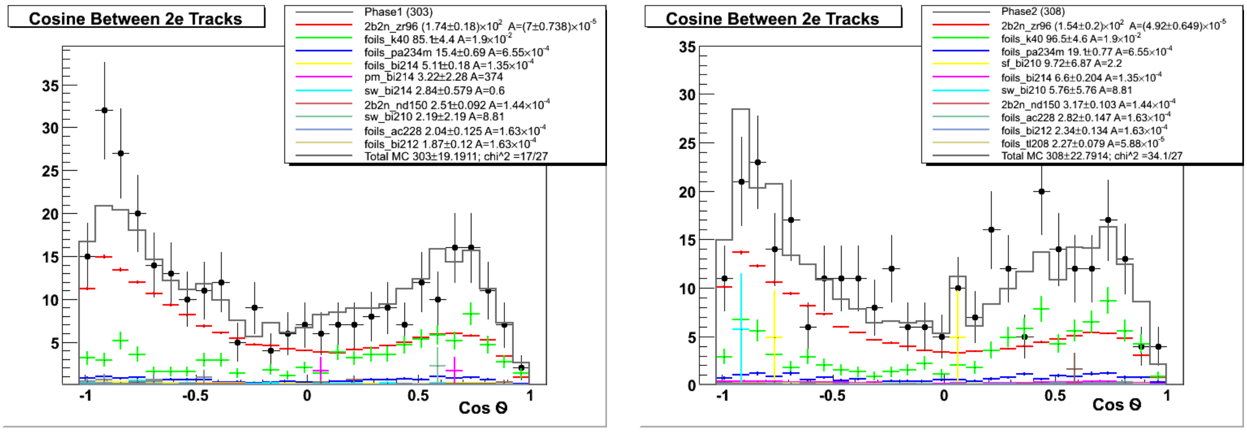

Figure 4.5 Phase-1 on the left and Phase-2 on the right. This plot is the cos θ between the two $\beta\beta$ tracks being emitted.

Looking at the single electron energy is also useful because any prominent peaks would be in indication of a single electron decay going to Moller (figure 4.6).

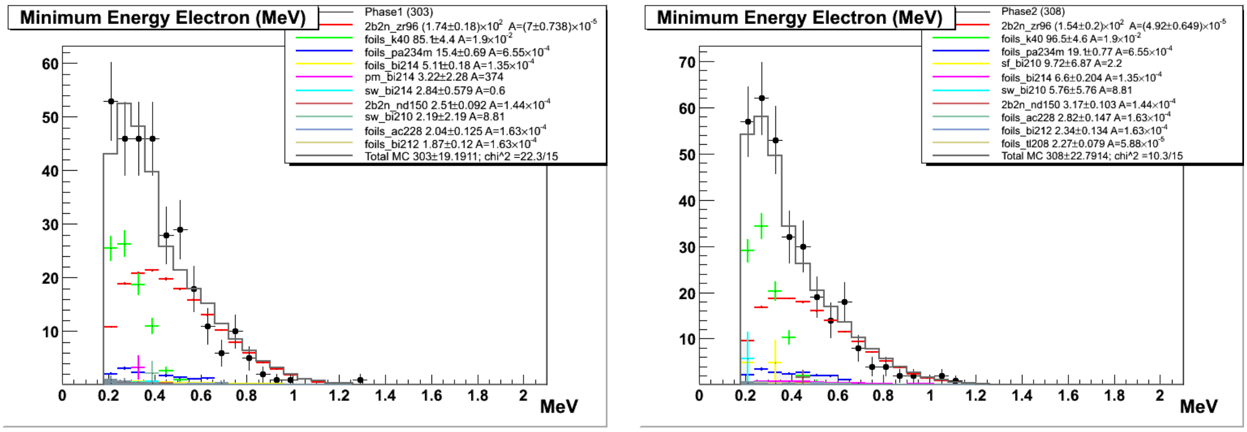

Figure 4.6 Phase-1 on the left and Phase-2 on the right. This is a plot of the minimum energy electron distribution.

From figure 4.3 and 4.4 we have a surplus of low energy data events < 1MeV because some low energy background remains to be realized. Provisionally, by making an energy cut we can ignore these low energy events and fit the high energy part of the spectrum that we understand. It is useful to make cuts at many different energies and observe how the half-life depends on the energy cut used. Below is a table of energy cuts and the resulting half-lives (table 4.7).

Energy Cut (MeV)	Phase-1 Half-Life 10e19 Yrs	error x10e19	Phase-2 Half-Life 10e19 Yrs	error x10e19	significance sigma
0.4	1.85	0.20	2.63	0.35	1.93
0.8	2.02	0.21	2.53	0.27	1.49
0.9	2.06	0.21	2.44	0.23	1.22
1.0	2.06	0.20	2.58	0.25	1.62
1.1	2.05	0.20	2.71	0.28	1.92
1.2	1.94	0.19	3.13	0.36	2.92
1.5	2.17	0.29	3.20	0.46	1.89

Table 4.7 Shows the dependence of the half-life measurement on the energy cut being made.

From table 4.7 it is easy to see that the measured half-life has a dependence on the energy cut being used. This is not the ideal situation and indicates that some systematic errors need to be realized. Ideally if all backgrounds are correctly known and modeled, there should be no dependence of the half-life measurement on the energy cut being made. Furthermore, phase-2 has a more dramatic dependence on the energy cut being used. The statistical significance between phase-1 and phase-2 is $\sim 2\sigma$ and could be claimed as a statistical fluctuation but this will be invested further because there are two candidates that fit the profile of the missing events, specifically Pb211 and Tl207, which both have an energy spectrum similar to K40.

4.4.4.3 NEMO-2 Results

The NEMO-2 experiment published its results after 0.084 mol years of Zr96 [**13**] and measured the $2\beta 2\nu$ half-life to be 2.1+0.8(stat)-0.4(stat)+/-0.2(syst) x10^{19} years. Their result is dominated by statistical error. My measured half-lives for phase-1 and phase-2 are <1.5σ from the NEMO-2 published result.

4.4.4.4 Conclusions

The analysis is far from complete and much work still lies ahead. Instead of using a pre-existing background model, I will be looking in the electron and electron plus gamma channels to make an independent measurement of the background contaminants. After many failed attempts, there is still a problem with the event counts for phase-1 and phase-2 not scaling proportionally. The run-time for phase-2 is $\sim$1/3 longer than for phase-1 and yet I have about the same number of events for both phases. Furthermore, the high radon levels in phase-1 are not adequate to explain this discrepancy. Lastly there is a slight difference from where the Zr96 foil is and where the MC thinks the foil is, so further analysis must be done to fine-tune the geometrical cuts being used.

4.5 Future Plans

- determine independent background model for internal backgrounds of Zr96 instead of using a pre-existing background model
- study systematics of the analysis (energy cut dependence) to find systematic error of $2\beta 2\nu$ half-life
- do an analysis of the $2\beta 0\nu$ channel
- finalize a $2\beta 2\nu$ half-life result
- find limit for $2\beta 0\nu$ half-life
- The NEMO-3 collaboration will be publishing my results together with the results from the other isotopes so I'll be submitting a description of my analysis and results.

5 SuperNEMO Calorimeter Design Study

The other part of my progress over the past 8 months includes many calorimeter related tests for the eventual SuperNEMO experiment. SuperNEMO will be based on the same technologies as NEMO-3 but will accommodate 100kg of source. It is also planned to be a modular detector meaning that each module will be a self-contained and fully-operational detector. This allows for data to be taken immediately after the completion of the first module instead of waiting for the full detector to be completed. There will be 20 modules in total. One of the significant improvements to SuperNEMO will be the improved energy resolution. NEMO-3 has an energy resolution of ~14% dE/E FWHM at 1MeV. SuperNEMO will do much better, achieving ~7% dE/E FWHM at 1MeV. This is only achievable by using high quantum efficiency (QE) ~35% photomultiplier tubes (PMT's) and specially designed lightguides and reflective coatings to direct all light from the scintillator to the photo-cathode of the PMT.

The baseline design for SuperNEMO is to have either 8" or 10" PMT's (or larger) coupled to large scintillator blocks. The cathode window of large PMT's is preferred to be hemispherical for two main reasons. A flat window would require thick glass to withstand the vacuum and a large flat window causes poor timing resolution. We have two options at this point to consider. We can construct a lightguide that is concave on one side to couple to the convex PMT and flat on the other side to couple to the scintillator, or we can construct the scintillator to be concave on one side and flat on the other and couple the scintillator directly to the PMT. The benefit of using the lightguide is that the machining process is much easier and less scintillating material is used and that saves money. The benefit of just machining the scintillator to fit the PMT is that in theory we will get a better energy resolution. However, simulations have been done that show that if the coupling between the lightguide and PMT is good, there should be no energy resolution degradation [**10**]. I am currently pursuing this option by testing different PMT's, lightguides, and scintillators to find a solution that balances performance and cost.

5.1 Setup and Test Procedure

The general test setup and procedure is quite simple. There are 3 main components being tested. The PMT, the lightguide, and the scintillator all work together to yield the final energy resolution of the setup. The PMT is optically coupled to the lightguide and the lightguide is optically coupled to the scintillator. The lightguide and scintillator are both wrapped in either Teflon or mylar to reflect escaping light back to the PMT. The conversion electrons from a Bi207 source are directed towards the scintillator. The energy from the electrons is converted into light by the scintillator and the light is then directed towards the PMT by the lightguide. The energy spectrum from the conversion electrons is a delta function so any broadening of the energy peak is due to the resolution degradation from the scintillator, lightguide, and PMT. Bi207 is also a gamma emitter so 3 separate data runs are taken to isolate the conversion electron spectrum. The first run is a pedestal run to check the electronics offset going to the ADC. The next run is with the Bi207 source radiating the scintillator with its full spectrum. In the third run we place a 2mm aluminum disk between the scintillator and Bi207 source to absorb the conversion elections and only let gamma's pass through. A figure of the gamma spectrum normalized to the full spectrum can be seen below (figure 5.1).

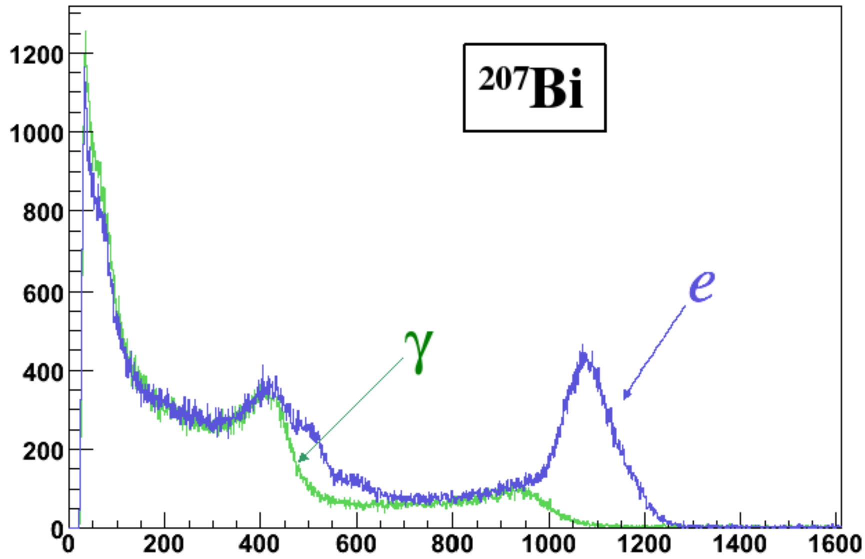

Figure 5.1 The two spectrum obtained from the Bi207 source without the beta shield (blue) and with the beta shield (green). The x-axis is in ADC bins and the y-axis is counts per bin.

5.2 Spectrum Analysis

Once the gamma spectrum has been subtracted from the full Bi207 spectrum, only the conversion electron spectrum remains (figure 5.2). The Bi207 spectrum has two main peaks at 482keV and 976keV. We are most interested in the 976keV peak because it is the most prominent peak. The 976keV peak is actually 3 Gaussian peaks (Gaussian because of photon statistics) from the K, L, and M electron shells of the isotope. When we fit the peak, we actually fit 3 overlapping peaks, so our fitting function takes this physics into account and then outputs the mean (μ) and sigma (σ) of the K-shell peak at 976keV. The other two peaks are at 1048keV and 1060keV. Because photon statistics dominate, the energy resolution can be approximated by:

$$dE/E = \sigma_{FWHM} \ / \ \mu$$

$$\sigma_{FWHM} = \sigma * 2.36$$

The number of photo-electrons (PE) can also be approximated by the ratio of:

$$PE = \mu^2 \ / \ \sigma^2$$

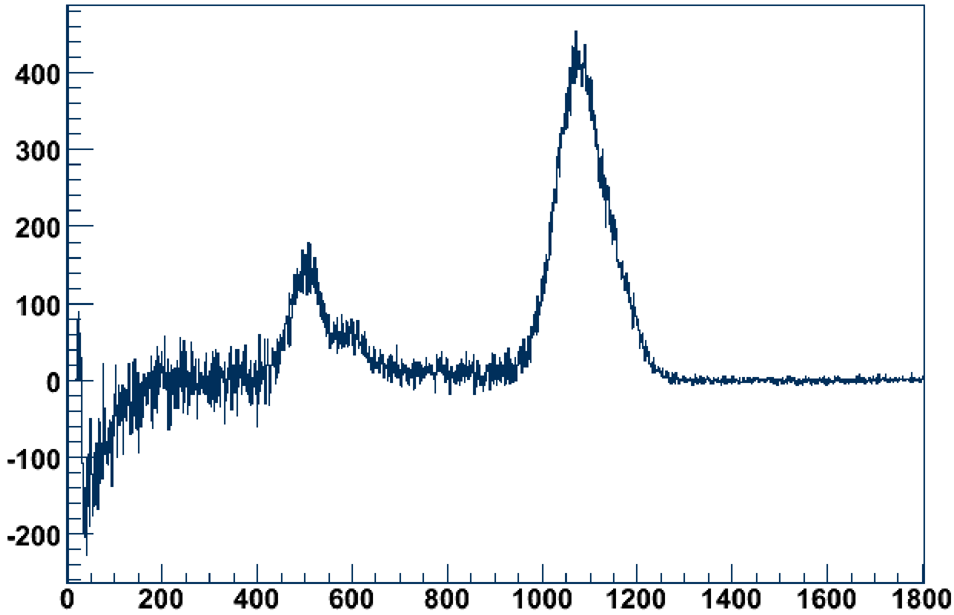

Figure 5.2 The remaining conversion electron spectrum after gamma spectrum subtraction. The x-axis is in ADC bins and the y-axis is counts per bin.

5.3 Light guide Tests

The most critical part of the PMT and lightguide configuration (as shown by simulations [**10**]) is the optical coupling of the lightguide to the PMT. An optical gel (Bicron BC-630) with index of refraction equal to 1.47 was initially tested to check the quality of the coupling. There were two main problems with the high viscosity gel. It was difficult for trapped air bubbles to escape from the coupled surface region and the large surface area made it difficult for the gel to fill in all the little imperfections of the machined surface of the lightguide. These factors lead to poor optical coupling and poor energy resolution. Figure 5.3.1 shows the gamma subtracted spectrum and the peak fit with a triple-Gaussian. The least χ^2 fit gives a resolution of 9.7% dE/E FWHM.

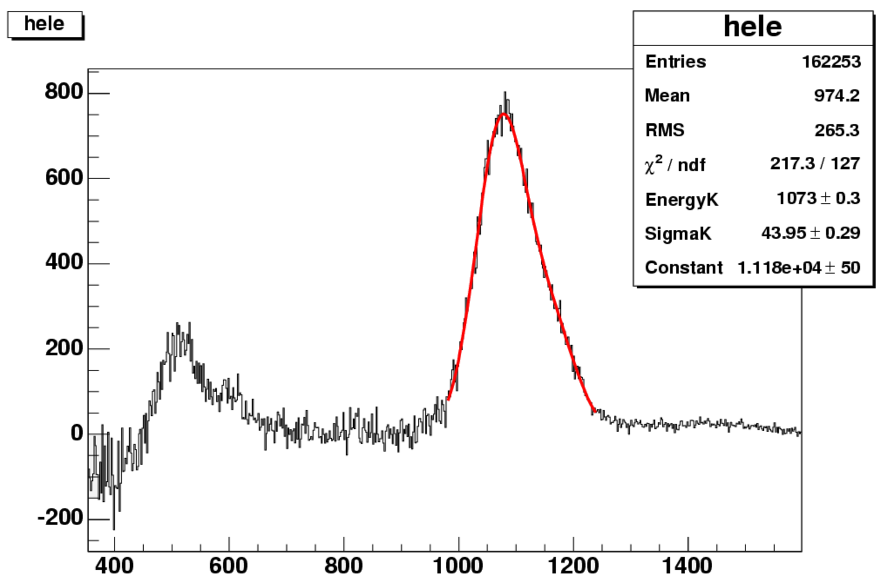

Figure 5.3.1 PMT and Lightguide coupled with viscus optical gel. The lightguide is wrapped in Teflon to reflect light back to the PMT. Pedestal and gamma spectrum are already subtracted out. Units on the x-axis are in ADC bins and on the y-axis are counts.

A less viscus optical gel (fluid) would increase the quality of coupling between the PMT and lightguide and one found was Cargille Laboratorie's fused silica matching-fluid, type 06350. Another factor to consider is the index of refraction for the PMT and lightguide. The PMT glass is around 1.54 and the lightguide is around 1.48 so an optical gel around 1.5 would be better. The optical gel previously used had an index of 1.465 but the type 06350 fluid has an index of 1.52 so this should improve the resolution. To my dismay, this new optical fluid did not improve the resolution as hoped. Two different reflective materials were used to wrap the lightguide. Mylar and Teflon are the leading competitors with Teflon being slightly better than Mylar in most cases. Below are the two results for the new optical fluid, one with a Mylar wrap and the other with the Teflon wrap (figure 5.3.2).

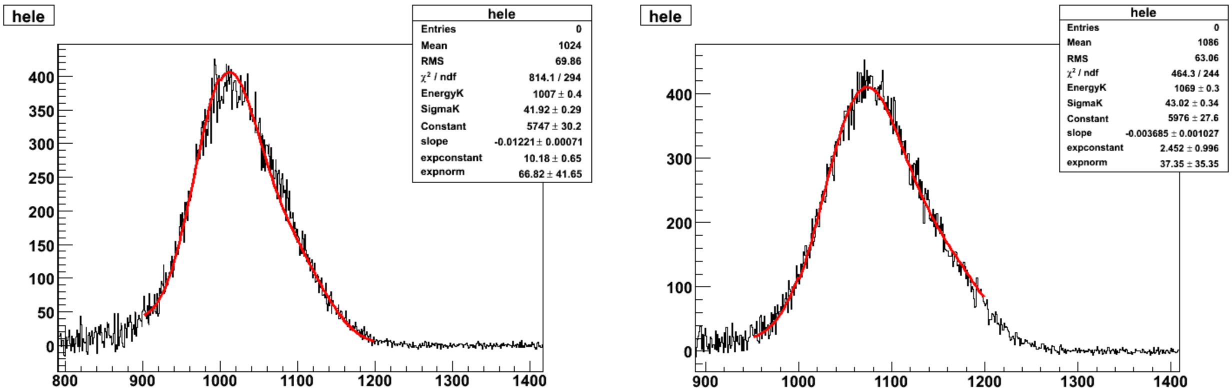

Figure 5.3.2 On the left is the Mylar test giving 9.8% dE/E and on the right is the Teflon test giving 9.5% dE/E.

Previous simulations showed that if good optical coupling was achieved, the lightguide should not degrade the resolution, so why was the resolution still so bad. One idea was that maybe the lightguide should not have a diffusively reflective surface around its circumference [**14**]. The reason for this is partly because of the lightguide's large volume and partly just as a test to see to what degree the resolution is effected. The circumference was polished and the tests were done again with both Mylar and Teflon wrappings (figure 5.3.3).

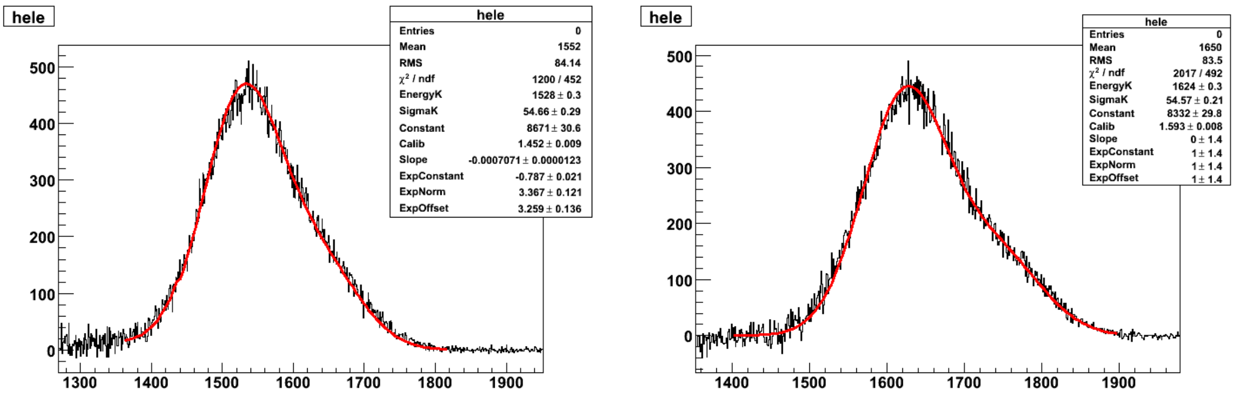

Figure 5.3.3 On the left is the Mylar giving 8.4% and on the right is the Teflon giving 8.0% dE/E FWHM. These tests are with the circumference of the lightguide polished.

Polishing the circumference of the lightguide improved the resolution by a full percent and this was long awaited good news. We're still one percent short of our 7% goal but a few ideas remain untested at this point.

5.4 Conclusions

Significant progress has been made and many options are left to be explored. The coupling of the PMT to the lightguide still remains somewhat of a question. To understand the lightguide better there are two tests that remain to be done. Firstly I plan to test the transmittance of the lightguide using an LED. The details have been left out but the point is that this measurement has not been done and the transmittance of the lightguide may not be what we expect ~100%. I also plan to test the wavelength dependence using a uniform light source and spectrometer because this has not been measured either. Previous tests done on the scintillators and their wavelength dependence proved to be quite different from the manufacturer's specifications [**15**]. A similar situation may apply to the lightguide as well.

5.5 Future Plans

- study the transmittance and wavelength dependence of the lightguide
- test new high QE PM's with lightguide and scintillator setup
- do light simulations for scintillator and lightguide to find where major losses are occurring
- do simulations of the setup with GEANT to predict resolution degradation
- I will be testing PMT's and scintillators to be used for the SuperNEMO prototype. The prototype will be used mainly to test the physics of the tracker and the timing information from the calorimeter is needed, therefore the resolution doesn't have to be perfect, but the timing must be fairly good. (a rise time of <5 nsec)

Thesis Evolution

This paper in itself provides the beginnings to my thesis. Many of the topics in this paper can be expanded upon in much greater detail. This paper provides a general outline that my thesis can use as its foundation. My thesis will contain much more data and results but will still be broken into two sections for the Zr96 analysis and calorimeter design study.

References

[1] D.Griffiths, Intro to Elementary Particles, John Wiley & Sons Inc., 1987
[2] S.M.Bilenky, physics/0603039 (2006)
[3] B.Kayser, hep-ph/0506165 (2005)
[4] C.Augier for NEMO Collaboration, LAL 05-162 (2005)
[5] M.Goeppert-Mayer, Phys. Rev. 48, 512-516 (1935)
[6] B.R.Martin, Nuclear and Particle Physics, John Wiley & Sons Inc., 2006
[7] E.Majorana, Nuovo Cimento 14, 171 (1937)
[8] W.H.Furry, Phys. Rev. 56, 1184-1193 (1939)
[9] S.Elliott and J.Engel, hep-ph/0405078 (2004)
[10] Vladimir Valsilyev, UCL London, private communications, 2007
[11] Vladimir Tretyak, INR Ukraine, private communications, 2007
[12] Victor Tretyak, JINR Dubna, Russia, private communications, 2007
[13] R.Arnold et al, Nucl. Phys. A 658, 299-312 (1999)
[14] Brain Anderson, UCL London, private communications, 2007
[15] Matthew Rose, UCL London, private communications, 2007

others

[16] R.Arnold et al, Nucl. Instr. and Meth. A 536, 79-122 (2005)
[17] K.N.Mukhin, Experimental Nuclear Physics: Vol 2, Mir Publishers, Moscow, 1987